SmB6 electron-phonon coupling constant from time- and angle-resolved photoelectron spectroscopy

Sterzi, A.; Crepaldi, A.; Cilento, F.; Manzoni, G.; Frantzeskakis, E.; Zacchigna, M.; van Heumen, E.; Huang, Y.K.; Golden, M.S.; Parmigiani, F.

DOI
10.1103/PhysRevB.94.081111

Publication date
2016

Document Version
Final published version

Published in
Physical Review B - Condensed Matter and Materials Physics

PHYSICAL REVIEW B **94**, 081111(R) (2016)

SmB_6 electron-phonon coupling constant from time- and angle-resolved photoelectron spectroscopy

A. Sterzi,[1] A. Crepaldi,[2,3,*] F. Cilento,[2] G. Manzoni,[1] E. Frantzeskakis,[4,5] M. Zacchigna,[6] E. van Heumen,[4] Y. K. Huang,[4] M. S. Golden,[4] and F. Parmigiani[1,2,7]

[1]*Universitá degli Studi di Trieste, Via A. Valerio 2, I-34127 Trieste, Italy*
[2]*Elettra-Sincrotrone Trieste S.C.p.A., Strada Statale 14, km 163.5, I-34149 Trieste, Italy*
[3]*Institute of Physics, Ecole Polytechnique Fédérale de Lausanne (EPFL), CH-1015 Lausanne, Switzerland*
[4]*Van der Waals-Zeeman Institute, Institute of Physics (IoP), University of Amsterdam, Science Park 904, NL-1098 XH Amsterdam, The Netherlands*
[5]*CSNSM, Université Paris-Sud, CNRS/IN2P3, Université Paris-Saclay, F-91405 Orsay, France*
[6]*CNR-IOM, Strada Statale 14, km 163.5, I-34149 Trieste, Italy*
[7]*International Faculty, University of Cologne, D-50937 Cologne, Germany*

(Received 9 May 2016; revised manuscript received 11 August 2016; published 25 August 2016)

SmB_6 is a mixed valence Kondo system resulting from the hybridization between localized f electrons and delocalized d electrons. We have investigated its out-of-equilibrium electron dynamics by means of time- and angle-resolved photoelectron spectroscopy. The transient electronic population above the Fermi level can be described by a time-dependent Fermi-Dirac distribution. By solving a two-temperature model that well reproduces the relaxation dynamics of the effective electronic temperature, we estimate the electron-phonon coupling constant λ to range from 0.13 ± 0.03 to 0.04 ± 0.01. These extremes are obtained assuming a coupling of the electrons with either a phonon mode at 10 or 19 meV. A realistic value of the average phonon energy will give an actual value of λ within this range. Our results provide an experimental report on the material electron-phonon coupling, contributing to both the electronic transport and the macroscopic thermodynamic properties of SmB_6.

DOI: 10.1103/PhysRevB.94.081111

The electronic transport properties of SmB_6 have been the subject of intense studies since the first report of its mixed valence nature [1] and the observation of a Kondo gap opening when cooling below $T_K \sim 50$ K [2]. This Kondo gap opens as a result of the interaction between the delocalized d electrons and the f electrons acting as localized magnetic impurities [3]. Despite the observation of a gap opening at the Fermi level by spectroscopic measurements, transport experiments show signs of residual conductivity [4]. The origin of this residual conductivity has puzzled the scientific community until the recent discovery of low-temperature metallic surface states [5], of potential, albeit debated, topological character [6–14].

The advent of topological insulators (TIs) has fueled the fast development of time- and angle-resolved photoelectron spectroscopy (tr-ARPES) [15–21]. This technique has been successfully exploited to access the unoccupied electronic states [22–24], as well as the temporal evolution of both the chemical potential (μ) and the electronic temperature (T_e) after optical excitation [16–19].

In this Rapid Communication we report on the out-of-equilibrium electronic properties of SmB_6 as revealed by tr-ARPES. This study is motivated by the possibility to address the scattering mechanisms in SmB_6, as similarly reported for Bi-based binary TIs [15,16,18–20]. Ishida and co-workers have pioneered this out-of-equilibrium approach to the study of SmB_6, reporting a shift of the chemical potential ($\Delta\mu$) lasting up to hundreds of μs after optical excitation, for $T < T_k$ [25]. By assessing the out-of-equilibrium dynamics of T_e, here we provide insights on the temporal evolution of the time-dependent Fermi-Dirac (FD) distribution. A minimal two-temperature model (2TM) is applied to mimic the relaxation dynamics of T_e. By considering a coupling to phonon energies corresponding to the lowest-energy Sm modes at 10 meV [26,27] or 19 [28] to 20 meV [27], we estimate an interval for the possible values of the electron-phonon coupling constant λ: 0.13 ± 0.03 to 0.04 ± 0.01. This range is mostly determined by the fact that among the phonon modes detected for this material, those derived from the B_6 cage, i.e., those at energies >20 meV, weakly contribute. This finding can be of relevance to account for the details of the electronic transport and thermodynamical properties of SmB_6 [29].

In addition to the temporal evolution of the FD function, we reveal a difference in the effect of the optical excitation on the d and f states. In particular, the depletion of intensity which follows the optical excitation is mainly located in the f bands. The electrons, which are excited in the f state above the Fermi level (E_F), successively relax towards E_F where intensity is observed over a broad momentum range. This suggests the transient population of empty f states above E_F [30].

Here, tr-ARPES experiments are performed at the T-ReX Laboratory, Elettra (Trieste, Italy); more details about the setup can be found in Refs. [17,31]. The photoelectrons are collected and analyzed by a SPECS Phoibos 225 hemispherical spectrometer, with energy and angular resolution set in the present experiment to 30 meV and 0.2° [17], respectively. The overall temporal resolution is equal to 250 fs. In the following, two data sets are analyzed with an absorbed fluence equal to 120 ± 25 and 75 ± 15 $\mu J/cm^2$, corresponding to an absorbed energy density equal to 30 ± 6 and 19 ± 4 J/cm^3, calculated by considering a penetration depth of 40 nm, as estimated from optical studies [32]. For the calculation of the absorbed fluence and energy density, a reflectivity $R = 0.5$ has been considered [32].

*alberto.crepaldi@epfl.ch

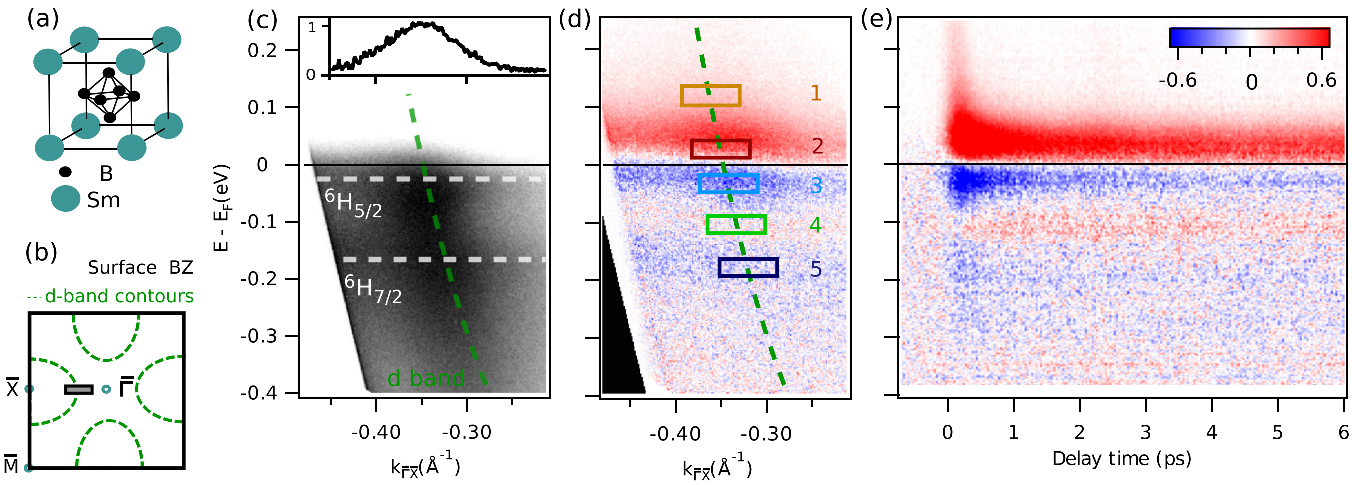

FIG. 1. (a) SmB_6 unit cell of the CsCl type. Sm atoms (teal) and a B_6 cage (black) occupy the corners and the body-centered position of the cubic cell. (b) Brillouin zone projected on the (001) cleavage plane. The measured momentum range along the $\bar{\Gamma}\bar{X}$ high symmetry direction is indicated by a gray rectangle. (c) Electronic properties measured at 120 K, 500 fs before optical excitation. Three spectral features are present, two nondispersive Sm f bands and a dispersive d-derived state, whose momentum distribution curve at E_F is shown in the inset. (d) Difference between the out-of-equilibrium electronic properties 300 fs after and 500 fs before optical excitation. Depletion of intensity (blue) is reveled only in the f state, and not in the d band. (e) Temporal evolution of the change in intensity along the d-band dispersion [green dashed line in (d)].

Single crystals of SmB_6 are grown via the optical floating zone technique, as described in Ref. [33]. They are cleaved in UHV at room temperature and transferred to a variable temperature cryostat. Measurements are performed at an equilibrium temperature of ~120 K. At this temperature the Kondo gap is fully closed and the material transport properties are metallic, a condition necessary for the use of a 2TM.

SmB_6 crystallizes in the CsCl-type structure with $Pm3m$ point group symmetry and lattice constant $a = 4.13$ Å. Sm atoms and a B_6 cage occupy the corners and the body-centered position of the cubic cell, as depicted in Fig. 1(a). Sample cleavage exposes the (001) surface, and the corresponding projected surface Brillouin zone is shown in Fig. 1(b). The tr-ARPES measurements have been carried out along the $\bar{\Gamma}\bar{X}$ high symmetry direction, in the region indicated by the gray rectangle. The d bands are expected to cross E_F within this momentum window, as illustrated by the green dashed lines schematizing the d-band contour [7–11,13].

Figure 1(c) shows the band structure at ~500 fs before optical excitation. Two nondispersive bands, traced by white dashed lines, are identified and attributed to the Sm $4f$-state multiplets $^6H_{5/2}$ and $^6H_{7/2}$ at binding energies of ~0.035 and ~0.180 eV, respectively. These flat states intersect a highly dispersive band derived from the Sm d orbitals, indicated by a dashed green line, crossing E_F at $k_F \sim 0.35$ Å^{-1}. The intensity of this state is found to be highly suppressed in s polarization, in agreement with the literature [9,13]. The momentum distribution curve (MDC) integrated in the energy window $E - E_F = 10 \pm 10$ meV [inset of Fig. 1(c)] shows the d-state peak, whose width is comparable with synchrotron-based measurements performed at higher photon energies (30–70 eV). The dispersion of the d band resembles results obtained for k_z far from the bulk high symmetry directions [9]. This is in agreement with our estimated $k_z \sim 2.7\pi/a$.

Figure 1(d) shows the modification of the electronic properties after optical excitation, for the highest absorbed energy density, resulting from the difference between the ARPES data 300 fs after and 500 fs before the arrival of the optical excitation. The color scale indicates with red (blue) the positive (negative) signal variation. The first noticeable feature, which characterizes the out-of-equilibrium electronic properties of SmB_6, is the different response of the two sets of bands to the optical excitation. A depletion of intensity (blue) is visible in the two nondispersive f states, whereas it is not observed along the dispersive d band. We ascribe this effect to the higher density of states (DOS) of the f state, which seems to dominate the optical absorption processes.

Since the experiments are performed at $T > T_K$ and E_F is crossed by the dispersive d band, we expect the material response to the optical excitation to be metallic. Hence, at short time scales immediately after optical excitation, electrons thermalize due to electron-electron scattering and relax towards E_F where their distribution is described by a time-dependent FD function [15–17,34–36]. This process is assumed to occur within the pump pulse duration [35,36]. Figure 1(d) shows that, after thermalization, electrons occupy a broad momentum region above E_F, thus suggesting the possible existence of unoccupied nondispersing f-like states above E_F [30]. The aim of our work is to evaluate the electron-phonon coupling constant from the temporal evolution of T_e, thus in the following we will focus only on the out-of-equilibrium dynamics of the time-dependent effective FD distribution, without entering in the details of the dispersion of the unoccupied states.

In order to estimate the time scale over which the electronic temperature relaxes, we now turn our attention to the temporal evolution of the ARPES signal. Figure 1(e) shows the temporal evolution of the change in photoemission intensity integrated along the dashed green line in Fig. 1(d). In order

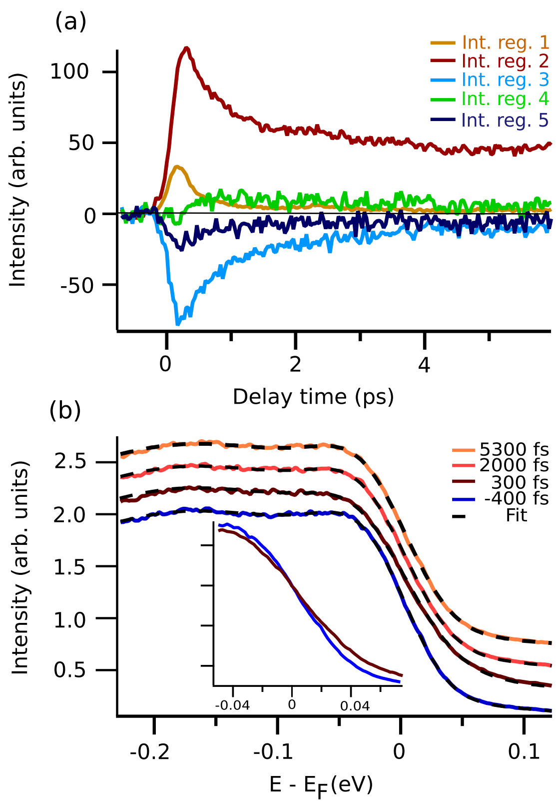

FIG. 2. (a) Nonequilibrium dynamics as obtained by integrating the recorded intensity within selected energy regions along the d-band dispersion. The color code is the same of the rectangles shown in Fig. 1(d). Regions 2 and 3, located symmetrically around E_F, display a similar characteristic time scale. Region 4, between the f states, is characterized by a small positive and delayed dynamics, different with respect to the negative dynamics of the f states in regions 3 and 5. (b) Energy distribution curves along the d-band dispersion at selected delay times before (−400 fs) and after (+300, +2000, +5300 fs) optical excitation. Black dashed lines indicate the best fit. The inset shows a zoom at E_F of the EDCs at −400 and +300 fs.

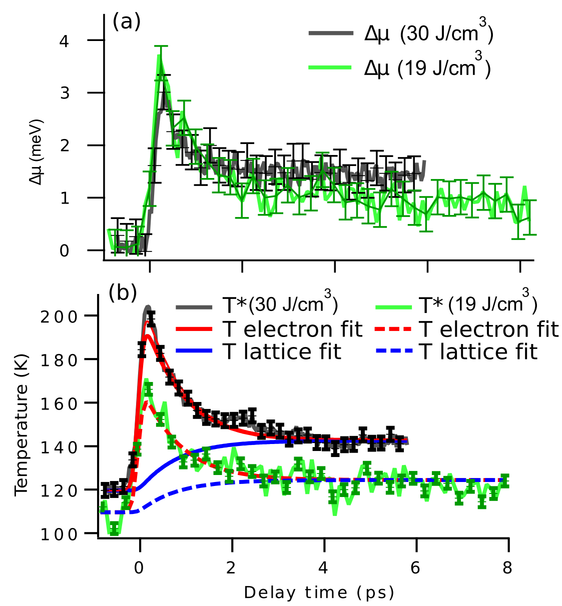

FIG. 3. (a), (b) Temporal evolution of the chemical potential shift $\Delta\mu$ and of the electronic temperature T_e, as obtained from the fit of the EDCs extracted from Fig. 1(e). The results for two excitation energy densities are shown, equal to $\sim 30 \pm 6$ J/cm^3 (black) and $\sim 19 \pm 4$ J/cm^3 (green). Both $\Delta\mu$ and T_e relax after optical excitation with a single exponential behavior, with a characteristic time $\tau =$ 800 ± 50 fs. The evolution of T_e is modeled within a 2TM, and the best fit is shown in (b). Red and blue lines indicate the dynamics of the electron and lattice temperature, respectively.

to quantitatively describe the characteristic relaxation times, traces are extracted from Fig. 1(e) in representative regions of the band structure, within the energies indicated by the colored rectangles. Figure 2(a) displays the resulting traces.

Region 1 (orange), at $E - E_F \sim 0.125$ eV, is characterized by a peak whose relaxation dynamics is comparable to our experimental temporal resolution. This prevents us from accessing the fast electronic dynamics responsible for the thermalization processes. At energies closer to E_F the dynamics slows down, as expected in a thermalized electron system [17,21]. The intensity relaxes to a plateau value larger than the equilibrium one. The full relaxation of the excited population is obtained through a second relaxation channel, having a time scale exceeding that achievable by the present experiment. From a single exponential fit to the traces, we observe that the relaxation dynamics in proximity of E_F has the same characteristic time $\tau = 800 \pm 50$ fs both above (region 2, brown) and below (region 3, light blue) E_F. This points to the fact that the dynamics is dominated by the thermal broadening of the FD distribution. The positive dynamics of region 4 (green), between the f multiplets, is delayed, and we ascribe this finding to a thermal broadening of the f states, rather than a purely electronic effect. This point will be clarified later within the frame of the 2TM.

In order to evaluate the evolution of the electronic temperature T_e, as well as of the chemical potential shift $\Delta\mu$, we fit a time-dependent FD function to the energy distribution curves (EDCs) extracted from Fig. 1(e) for all the delay times. Figure 2(b) shows selected EDCs at −400, +300, +2000, and +5300 fs, vertically offset for clarity, along with the corresponding fits (black dashed lines). The broadening of the FD distribution is more clearly visible in the inset, which shows a zoom at E_F of the two EDCs at −400 and +300 fs. The fitting function results from the convolution of a Gaussian function, accounting for the experimental energy resolution, with the result of the product of a time-dependent FD distribution and a function describing the density of states [16]. In the present study, the latter is the sum of two Lorentzian components for the f multiplets in the occupied density of states, at −0.18 and −0.035 eV, and a constant accounting for the DOS of the d band. In performing the fit of the experimental EDCs, we only let T_e and $\Delta\mu$ vary with time. The reason for letting free only two fitting parameters is phenomenological: The parameters in the density-of-states function, when allowed to vary, do not produce an improvement of the χ^2 of the fit.

Figures 3(a) and 3(b) show the dynamics of $\Delta\mu$ and T_e, respectively. Results are reported for both data sets, with excitation energy densities equal to 30 ± 6 J/cm^3 (black) and 19 ± 4 J/cm^3 (green). After optical excitation, both $\Delta\mu$ and T_e relax with a single exponential behavior, with a similar characteristic time $\tau = 800 \pm 50$ fs. The values of $\Delta\mu$ are small but comparable with the previous work of Ishida *et al.* [25]. However, we point out that in the present study we are not sensitive to the surface photovoltage effect which is expected to slow the $\Delta\mu$ relaxation dynamics for $T < T_K$ [25]. The fact that the relaxation of T_e is well mimicked by a single decaying exponential justifies the choice of a minimal 2TM for extracting λ. The evolution of the electron and lattice temperatures (T_l) is described by the following rate equations [36,37]:

$$\frac{\partial T_e}{\partial t} = \frac{S(t)}{C_e} - \frac{3\lambda\Omega^3(n_e - n_l)}{\hbar\pi k_b^2 T_e}, \tag{1}$$

$$\frac{\partial T_l}{\partial t} = \frac{C_e}{C_l}\frac{3\lambda\Omega^3(n_e - n_l)}{\hbar\pi k_b^2 T_e}. \tag{2}$$

$S(t)$ describes the optical excitation with a Gaussian profile and absorbed energy density equal to $\sim 30 \pm 6$ and $\sim 19 \pm 4$ J/cm^3, respectively. The error bar associated with the energy density propagates into an error bar on the free fitting parameters in the 2TM, including λ. Ω corresponds to the phonon frequency. From optics, neutron scattering, and symmetry analysis we expect only phonon modes at 10 meV (acoustic) [26,27], 19–20 meV [27,28] (T_{1u}), and three higher energies vibrational and rotational modes of the B_6 cage at 89.6 meV (T_{2g}) and 141.7 meV (E_g) and 158.3 meV (A_{1g}) [26]. In the Eliashberg formalism, λ results from the coupling of all the phonon modes, where the contribution from each mode is divided by its phonon energy. For this reason we expect the coupling to the high-energy B_6 modes to be weak. This hypothesis is well supported by analogy with the calculations performed on a similar compound, YB_6, which show that the electron-phonon coupling constant λ is dominated by the low-energy Y phonon modes, while the high-energy phonons associated with the B_6 modes only weakly contribute to λ [38].

For these reasons, we have performed our analysis by considering the coupling to the low-energy Sm modes at 10 meV [26,27] and 19 [28] to 20 meV [27], respectively. k_b is the Boltzmann constant and n_e and n_l are the Bose-Einstein (BE) distribution functions for phonons calculated at temperatures T_e and T_l, respectively. In the model we assumed a particular form for the electron-phonon coupling, i.e., $\alpha^2 F(\omega) \propto \delta(\omega - \Omega)$, but no approximations are applied to the BE statistics. This is because the measured electronic temperature is not high enough to justify the commonly used "high-temperature" approximation of the BE statistics [37]. The lattice specific heat C_l for a lattice base temperature of 120 K (110 K for 19 ± 4 J/cm^3) is taken from Ref. [29], while the electronic specific heat is $C_e = \gamma T_e$, with γ left free to vary as well as λ.

The best fit to T_e is shown by the continuous and dashed red lines in Fig. 3(b), for the two excitation energy densities, respectively, whereas blue lines indicate the dynamics of T_l. The electronic and lattice temperatures equilibrate after approximately 2 ps, and T_l is expected to recover its equilibrium value through lattice heat diffusion on time scales longer than the temporal window of our measurements [36]. The 2TM well reproduces the evolution of T_e, thus indicating that mechanisms, such as electronic heat diffusion, do not need to be taken into account for the case of the bad metal SmB_6, in contrast to conventional metals such as Ru(001) [39] and Gd(0001) [40]. The increase in T_l accounts for the long lasting plateau observed in the dynamics across E_F in regions 2 and 3 in Fig. 2(a). The increase in T_l is delayed with respect to the optical excitation, as it turns out from the 2TM. This suggests a possible interpretation for the positive dynamics of region 4 in Fig. 2(a), whose maximum is reached at a later time than that of the other regions, as a consequence of thermal broadening of the f multiplets due to the larger T_l. From the model we estimate a value of γ equal to 5.8 ± 1.5 mJ/mol K^2, in good agreement with the literature, where values of 7 mJ/mol K^2 [41] and 2 mJ/mol K^2 [42] are found.

Finally, an important result of our analysis is the evaluation of the electron-phonon coupling constant. From the 2TM, by considering the coupling dominated by the low-energy Sm phonons, either with $\Omega = 10$ meV [26,27] or $\Omega = 19$ meV [28] to 20 meV [27], we obtain a value of $\lambda\Omega^3$ equal to 130 ± 30 or 270 ± 70 meV^3, respectively. From these we extract two extreme values for λ equal to 0.13 ± 0.03 and 0.04 ± 0.01. We can conclude that, for a realistic value of the average phonon energy between 10 and 19–20 meV, depending on the phonon density of states, λ will lie between 0.13 ± 0.03 and 0.04 ± 0.01. Unfortunately, no theoretical or experimental estimations of λ are available for SmB_6 in the literature. From a comparison with different hexaborides, we note that the range in which λ falls for SmB_6 is slightly lower than those reported for LaB_6 ($\lambda = 0.17$–0.26 [43]), MgB_6 ($\lambda = 0.39$ [44]), and YB_6 ($\lambda = 0.86$ [45]).

Our estimation of λ provides an insight into a fundamental physical property of SmB_6. The slightly smaller value, compared to other hexaborides, might reflect an intrinsic difference in the electron-phonon coupling. Nonetheless, it might also be ascribed to the fact that tr-ARPES is momentum selective. We point out that the λ value is evaluated along the $\bar{\Gamma}\bar{X}$ high symmetry direction, and far from the zone boundary, owing to the small momentum window accessible with the available photon energy. We believe that our results represent a reference for future momentum integrated measurements of λ that might extend further the comparison between the electron-phonon coupling in different hexaboride compounds.

In conclusion, we have exploited tr-ARPES to investigate the out-of-equilibrium electronic properties of SmB_6. After optical excitation, electrons are transferred predominantly from the localized f multiplets to the unoccupied density of states. After thermalization, electrons can be described by a time-dependent Fermi-Dirac distribution. The temporal evolution of the electronic temperature is described within a minimal two-temperature model. The phonon density of states is unknown for SmB_6, hence we can establish a range of values for λ. By assuming that the electron-phonon coupling, along the $\bar{\Gamma}\bar{X}$ direction of the surface BZ, is preferentially mediated by the two lowest-energy Sm modes at 10 meV [26,27] or 19 [28] to 20 meV [27], we estimate λ to fall in the range 0.13 ± 0.03 to 0.04 ± 0.01.

This work was supported in part by the Italian Ministry of University and Research under Grants No. FIRBRBAP045JF2 and No. FIRB-RBAP06AWK3 and by the European Community Research Infrastructure Action under the FP6 "Structuring the European Research Area" Program through the Integrated Infrastructure Initiative "Integrating Activity on Synchrotron and Free Electron Laser Science", Contract No. RII3-CT-2004-506008. This work has been partially funded by the research programme of the Foundation for Fundamental Research on Matter (FOM), which is part of the Netherlands Organization for Scientific Research (NWO). We are grateful to X. Zhang and co-workers for the provision of single crystals in the initial stage of this study.

A.S. and A.C. contributed equally to this work.

[1] E. E. Vainshtein, S. M. Blokhin, and Yu. B. Paderno, Sov. Phys. Solid State **6**, 2318 (1965).

[2] J. W. Allen, B. Batlogg, and P. Wachter, Phys. Rev. B **20**, 4807 (1979).

[3] D. Malterre, M. Grioni, and Y. Baer, Adv. Phys. **45**, 299 (1996).

[4] J. C. Cooley, M. C. Aronson, Z. Fisk, and P. C. Canfield, Phys. Rev. Lett. **74**, 1629 (1995).

[5] G. Li, Z. Xiang, F. Yu, T. Asaba, B. Lawson, P. Cai, C. Tinsman, A. Berkley, S. Wolgast, Y. S. Eo *et al.*, Science **346**, 1208 (2014).

[6] M. Dzero, K. Sun, V. Galitski, and P. Coleman, Phys. Rev. Lett. **104**, 106408 (2010).

[7] M. Neupane, N. Alidoust, S.-Y. Xu, T. Kondo, Y. Ishida, D. J. Kim, C. Liu, I. Belopolski, Y. J. Jo, T.-R. Chang *et al.*, Nat. Commun. **4**, 2991 (2013).

[8] N. Xu, X. Shi, P. K. Biswas, C. E. Matt, R. S. Dhaka, Y. Huang, N. C. Plumb, M. Radović, J. H. Dil, E. Pomjakushina *et al.*, Phys. Rev. B **88**, 121102 (2013).

[9] E. Frantzeskakis, N. de Jong, B. Zwartsenberg, Y. K. Huang, Y. Pan, X. Zhang, J. X. Zhang, F. X. Zhang, L. H. Bao, O. Tegus *et al.*, Phys. Rev. X **3**, 041024 (2013).

[10] J. D. Denlinger, J. W. Allen, J.-S. Kang, K. Sun, J.-W. Kim, J. H. Shim, B. I. Min, D.-J. Kim, and Z. Fisk, arXiv:1312.6637.

[11] Z.-H. Zhu, A. Nicolaou, G. Levy, N. P. Butch, P. Syers, X. F. Wang, J. Paglione, G. A. Sawatzky, I. S. Elfimov, and A. Damascelli, Phys. Rev. Lett. **111**, 216402 (2013).

[12] N. Xu, P. Biswas, J. Dil, R. Dhaka, G. Landolt, S. Muff, C. Matt, X. Shi, N. Plumb, M. R. E. Pomjakushina *et al.*, Nat. Commun. **5**, 4566 (2014).

[13] P. Hlawenka, K. Siemensmeyer, E. Weschke, A. Varykhalov, J. Sánchez-Barriga, N. Y. Shitsevalova, A. V. Dukhnenko, V. B. Filipov, S. Gábani, K. Flachbart *et al.*, arXiv:1502.01542.

[14] S. Ramankutty, N. de Jong, Y. Huang, B. Zwartsenberg, F. Massee, T. Bay, M. Golden, and E. Frantzeskakis, J. Electron Spectrosc. Relat. Phenom. **208**, 43 (2016).

[15] J. A. Sobota, S. Yang, J. G. Analytis, Y. L. Chen, I. R. Fisher, P. S. Kirchmann, and Z.-X. Shen, Phys. Rev. Lett. **108**, 117403 (2012).

[16] Y. H. Wang, D. Hsieh, E. J. Sie, H. Steinberg, D. R. Gardner, Y. S. Lee, P. Jarillo-Herrero, and N. Gedik, Phys. Rev. Lett. **109**, 127401 (2012).

[17] A. Crepaldi, B. Ressel, F. Cilento, M. Zacchigna, C. Grazioli, H. Berger, P. Bugnon, K. Kern, M. Grioni, and F. Parmigiani, Phys. Rev. B **86**, 205133 (2012).

[18] A. Crepaldi, F. Cilento, B. Ressel, C. Cacho, J. C. Johannsen, M. Zacchigna, H. Berger, P. Bugnon, C. Grazioli, I. C. E. Turcu *et al.*, Phys. Rev. B **88**, 121404 (2013).

[19] M. Hajlaoui, E. Papalazarou, J. Mauchain, L. Perfetti, A. Taleb-Ibrahimi, F. Navarin, M. Monteverde, P. Auban-Senzier, C. Pasquier, N. Moisan *et al.*, Nat. Commun. **5**, 3003 (2014).

[20] J. Sobota, S.-L. Yang, D. Leuenberger, A. Kemper, J. Analytis, I. Fisher, P. Kirchmann, T. Devereaux, and Z.-X. Shen, J. Electron Spectrosc. Relat. Phenom. **195**, 249 (2014).

[21] C. Cacho, A. Crepaldi, M. Battiato, J. Braun, F. Cilento, M. Zacchigna, M. C. Richter, O. Heckmann, E. Springate, Y. Liu *et al.*, Phys. Rev. Lett. **114**, 097401 (2015).

[22] J. Sobota, S.-L. Yang, A. Kemper, J. Lee, F. Schmitt, W. Li, R. Moore, J. Analytis, I. Fisher, P. Kirchmann *et al.*, Phys. Rev. Lett. **111**, 136802 (2013).

[23] J. C. Johannsen, G. Autès, A. Crepaldi, S. Moser, B. Casarin, F. Cilento, M. Zacchigna, H. Berger, A. Magrez, P. Bugnon *et al.*, Phys. Rev. B **91**, 201101 (2015).

[24] G. Manzoni, A. Sterzi, A. Crepaldi, M. Diego, F. Cilento, M. Zacchigna, P. Bugnon, H. Berger, A. Magrez, M. Grioni *et al.*, Phys. Rev. Lett. **115**, 207402 (2015).

[25] Y. Ishida, T. Otsu, T. Shimada, M. Okawa, Y. Kobayashi, F. Iga, T. Takabatake, and S. Shin, Sci. Rep. **5**, 8160 (2015).

[26] P. A. Alekseev, B. D. A. S. Ivanov, H. Schober, A. S. M. K. A. Kikoin, V. N. Lazukov, E. S. Konovalova, Y. B. Paderno, A. Y. Rumyantsev, and I. P. Sadikov, Europhys. Lett. **10**, 457 (1989).

[27] M. E. Valentine, S. Koohpayeh, W. A. Phelan, T. M. McQueen, P. F. S. Rosa, Z. Fisk, and N. Drichko, Phys. Rev. B **94**, 075102 (2016).

[28] A. Tytarenko, E. van Heumen *et al.* (unpublished).

[29] W. A. Phelan, S. M. Koohpayeh, P. Cottingham, J. W. Freeland, J. C. Leiner, C. L. Broholm, and T. M. McQueen, Phys. Rev. X **4**, 031012 (2014).

[30] F. Lu, J. Z. Zhao, H. Weng, Z. Fang, and X. Dai, Phys. Rev. Lett. **110**, 096401 (2013).

[31] F. Cilento, A. Crepaldi, G. Manzoni, A. Sterzi, M. Zacchigna, P. Bugnon, H. Berger, and F. Parmigiani, J. Electron Spectrosc. Relat. Phenom. **207**, 7 (2016).

[32] G. Travaglini and P. Wachter, Phys. Rev. B **29**, 893 (1984).

[33] L. H. Bao, O. Tegus, J. X. Zhang, X. Zhang, and Y. K. Huang, J. Alloys Compd. **558**, 39 (2013).

[34] J. C. Johannsen, S. Ulstrup, F. Cilento, A. Crepaldi, M. Zacchigna, C. Cacho, I. C. E. Turcu, E. Springate, F. Fromm, C. Raidel *et al.*, Phys. Rev. Lett. **111**, 027403 (2013).

[35] W. S. Fann, R. Storz, H. W. K. Tom, and J. Bokor, Phys. Rev. B **46**, 13592 (1992).

[36] L. Perfetti, P. A. Loukakos, M. Lisowski, U. Bovensiepen, H. Eisaki, and M. Wolf, Phys. Rev. Lett. **99**, 197001 (2007).

[37] P. B. Allen, Phys. Rev. Lett. **59**, 1460 (1987).

[38] Y. Xu, L. Zhang, T. Cui, Y. Li, Y. Xie, W. Yu, Y. Ma, and G. Zou, Phys. Rev. B **76**, 214103 (2007).

[39] M. Lisowski, P. Loukakos, U. Bovensiepen, J. Stahler, C. Gahl, and M. Wolf, Appl. Phys. A **78**, 165 (2004).

[40] U. Bovensiepen, J. Phys.: Condens. Matter **19**, 083201 (2007).

[41] T. Kasuya, K. Takegahara, T. Fujita, T. Tanaka, and E. Bannai, J. Phys. (Paris) **40**, 308 (1979).

[42] S. von Molnar, T. Theis, A. Benoit, A. Briggs, J. Floquet, J. Ravex, Z. Fisk, P. Watcher, and H. Boppart, *Valence Instabilities* (North-Holland, Amsterdam, 1982), p. 389.

[43] Yu. S. Ponosov and S. V. Strel'tsov, JETP Lett. **97**, 447 (2013).

[44] H. Wang, K. A. LeBlanc, B. Gao, and Y. Yao, J. Chem. Phys. **140**, 044710 (2014).

[45] J. Teyssier, A. Kuzmenko, D. van der Marel, R. Lortz, A. Junod, V. Filippov, and N. Shitsevalova, Phys. Status Solidi C **3**, 3114 (2006).